引用格式：LUO Guoping, CHEN Xingyuan, HU Sumei, et al. Near Infrared Hot Electrons Photodetectors Based on Tamm Plasmons[J]. Acta Photonica Sinica, 2022, 51(4):0404002
罗国平,陈星源,胡素梅,等.基于塔姆等离激元的近红外热电子光电探测器[J].光子学报,2022,51(4):0404002

基于塔姆等离激元的近红外热电子光电探测器

罗国平,陈星源,胡素梅,朱伟玲
(广东石油化工学院 理学院,广东 茂名 525000)

摘　要:提出了一种实现高性能宽带近红外热电子光电探测器的多层薄膜器件结构,该结构基于TiN/TiO_2肖特基势垒和TiN/分布式布拉格反射器形成的塔姆等离激元。通过光学传输矩阵和热电子发射理论模拟计算结果表明,高折射率比介质层构成的分布式布拉格反射器有效扩展了TiN薄膜吸收光谱和器件响应光谱,同时增强了TiN薄膜的吸收率和器件响应度。通过调控分布式布拉格反射器结构参数、TiN薄膜厚度和MgF减反射层厚度,可获得高达29.2 mA/W的响应度,响应光谱半峰全宽约为900 nm,为高性能宽带近红外热电子器件的实现提供了新的途径,有利于拓展热电子光电探测器的应用领域。

关键词:光电探测器;热电子;等离激元;量子效率;薄膜
中图分类号:TN202　　**文献标识码**:A　　**doi**:10.3788/gzxb20225104.0404002

0　引言

光探测是现代检测技术和智能传感的重要手段和方法。经典的光电探测器基于半导体材料电子的带间跃迁,其最大响应波长取决于半导体材料的光学禁带,只有能量大于光学禁带(波长小于最大响应波长)的光子才能被探测[1]。红外光电探测器广泛应用于军事侦察、航天遥感、天文观测、工业探测、光纤通信、红外成像等领域[2-4]。常见的红外探测器采用光学禁带极窄的半导体材料制作而成,面临着工艺复杂、成本高昂、低温工作等诸多问题[5]。基于内光电效应的热电子光电探测器因其能够突破半导体材料最大响应波长的限制、避免能量弛豫损失、响应速度快、可室温环境工作、偏振敏感等优点在过去的十多年引起了国内外研究者的广泛关注[6-9]。热电子光电探测器面临的主要问题是响应度低,特别是在近红外波段。近年来,国内外研究者在近红外热电子光电探测器制备与器件光电性能提升方面做了许多研究,通过光栅等离激元[10-11]、塔姆(Tamm)等离激元[12-13]和微腔效应[14]等光学手段可以有效增强热电子光电探测器中金属薄膜的光吸收率,进一步提高器件的响应度。基于平面金属薄膜/分布式布拉格反射器(Distributed Bragg Reflector, DBR)的塔姆等离激元具有结构简单、制造成本低、吸收效率高等优点。通过调节DBR结构参数和金属薄膜厚度,可以调控塔姆等离激元共振波长。这种结构提供了一种提高热电子光电探测器吸收率的有效途径,然而相应器件通常表现出窄带吸收和窄带响应的特性[15-16]。开发宽带响应特性的热电子光电探测器有利于扩展其在光纤通信、光催化、太阳能电池、太阳能水分解等领域的应用[17-19]。在宽带热电子光电探测器研究方面,国内外研究者也做了一些探索。贺涛研究员等研制了金-硅超表面的双波段响应热电子光电探测器,无偏压下可见光和近红外波段的响应度分别为7 mA/W和3 mA/W[20]。王琦龙教授等通过化学湿法刻蚀和真空蒸镀技术制备了金薄膜覆盖硅微金字塔型近红外光电探测器,研究了不同金薄膜厚度对器件光电性能的影响,在1 310 nm波长处的响应度达到1.8 mA/W[21]。王志明教授等设计了TiN/n-Si/DBR的宽带热电子光电探测器,研究了TiN薄膜厚度、DBR中心波长、入射光角度等对器件光吸收率和响应度的影响[22]。他们使用的DBR由周期性TiO_2/Al_2O_3构成,器件吸收光谱半峰全宽(Full Width at Half

基金项目:国家自然科学基金(No.12074441),广东省科技计划(Nos. 2018A03030728, 2019A1515010916),广东省教育厅青年创新人才项目(No. 2017KQNCX136),广东石油化工学院科研基金(No. 2017rc20)
第一作者:罗国平(1988—),男,讲师,博士,主要研究方向为光电材料与器件。Email: guopingluo@126.com
收稿日期:2021-10-12;**录用日期**:2021-12-01

Maximum，FWHM）为239.3 nm，最高吸收率为94.2%。SAKHDARI M等研究了多层Ag-TiO_2构成的双曲型超材料的热电子器件光电性能。理论计算表明该结构能实现宽光谱高响应度，并且与入射角无明显关系[23]。SHINDE S L等制备了TiN/Ge热电子光电探测器，在1 800～2 600 nm波段响应度几乎保持不变，约为40 pA/mW[24]。就宽带热电子光电探测器而言，还存在着器件宽带光吸收率不高、响应光谱范围窄、响应度低等亟待解决的难题[25-27]。

TiN在近红外波段具有较高的介电常数和优良的等离激元特性[28-29]。TiN薄膜中热电子的平均自由程约为50 nm，大于Au和Ag的值[30]。因此，TiN被视为实现高性能宽带热电子光电探测器的候选材料[31-32]。在本研究中，提出了一种多层薄膜结构以实现高性能宽带近红外热电子光电探测器。该结构具有以下特点：1）调整DBR结构参数的TiN/DBR塔姆等离激元能够增强TiN薄膜的宽带吸收率并拓宽器件吸收光谱和响应光谱；2）TiN与TiO_2之间的肖特基势垒仅为0.37 eV，有利于低能热电子的输运[33]；3）引入MgF减反射层，减少入射光损耗，最大吸收率接近100%。

1 模型与方法

图1(a)为宽带近红外热电子光电探测器多层薄膜结构示意图。入射光从上侧入射沿着z轴传输，在传输方向上分别通过MgF、ITO、TiO_2、TiN和DBR。其中MgF为减反射层，ITO为透明电极，TiO_2为半导体层，TiN为光吸收层，TiO_2/TiN构成肖特基势垒。DBR由光程为四分之一波长的高折射率和低折射率介质层周期性堆叠组成。图1(b)展示了宽带近红外热电子光电探测器的工作机理[34]：1）入射光经塔姆等离激元被TiN薄膜吸收，从而产生热电子；2）获得一定动能的热电子向TiN/TiO_2肖特基势垒界面输运；3）具有足够能量的热电子越过TiN/TiO_2肖特基势垒注入到TiO_2薄膜。热电子在TiO_2薄膜传输后最终被ITO透明电极收集，器件可在零偏压下工作。

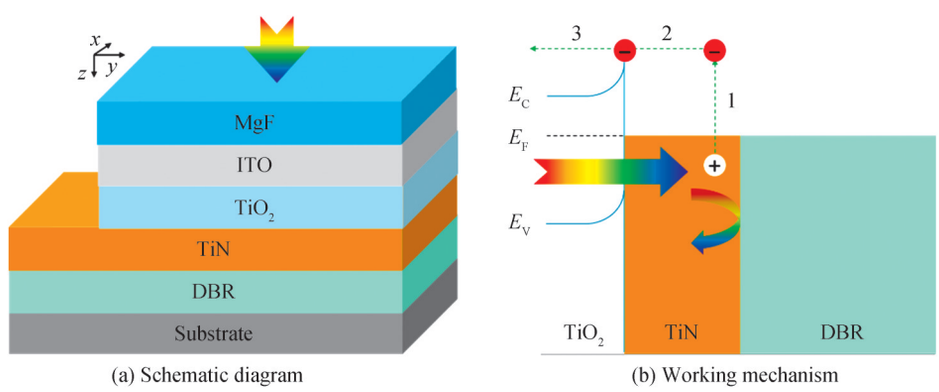

图1 多层薄膜结构宽带近红外热电子光电探测器结构和工作机理示意图

Fig.1 Schematic diagram and working mechanism of the broadband near infrared hot electrons photodetector with multi-layer structure

热电子光电探测器的响应度R可以表示为[35]

$$R(h\nu)=A(h\nu)P(h\nu)D(h\nu) \tag{1}$$

式中，h为普朗克常数，ν为入射光子频率，$A(h\nu)$为热电子的产生率（外量子效率，EQE），$P(h\nu)$为热电子输运到达TiN/TiO_2肖特基势垒界面的概率（输运概率），$D(h\nu)$为热电子越过TiN/TiO_2肖特基势垒注入到TiO_2薄膜的概率（注入概率）。内量子效率（IQE）为$P(h\nu)$和$D(h\nu)$的乘积。

热电子的产生率计算公式为[36]

$$A(h\nu)=\frac{\iiint_V(1-P_r)\pi\varepsilon_i\left|E(z,h\nu)\right|^2\mathrm{d}V}{h} \tag{2}$$

式中，P_r为局域电阻损耗常数（～25%），ε_i为TiN薄膜的介电常数，$E(z,h\nu)$为位置z处的光电场强度，由光学传输矩阵计算得到[37]。

热电子从产生处输运到达TiN/TiO_2肖特基势垒界面的概率为[38]

$$P(h\nu)=\frac{1}{2\pi}\int_0^{\pi}\exp\left[-\frac{d(z)}{\lambda_M(h\nu)|\cos(\theta)|}\right]\mathrm{d}\theta \tag{3}$$

式中，$d(z)$为热电子生成位置与肖特基势垒界面之间的垂直距离，$\lambda_M(h\nu)$为与能量相关的热电子平均自由程，θ为热电子的扩散角。

热电子穿过TiN/TiO_2肖特基势垒注入到TiO_2薄膜的概率由电子分布联合态密度（EDJDOS）理论[39]计算得出，即

$$D(h\nu)=\frac{\int_{\Phi_{BS}}^{h\nu}\rho(E,h\nu)\mathrm{d}E}{\int_0^{h\nu}\rho(E,h\nu)\mathrm{d}E} \tag{4}$$

式中，$\rho(E,h\nu)$为TiN薄膜的电子态密度，由热电子能量分布函数和费米-狄拉克分布函数所确定[39]

$$\rho(E,h\nu)=(E_e-h\nu)^{1/2}f(E_e-h\nu)E_e{}^{1/2}[1-f(E_e)] \tag{5}$$

式中，E_e为热电子的动能（$0<E_e<h\nu$），$f(x)$为费米-狄拉克分布函数。注入概率与热电子到达肖特基势垒界面时的能量和肖特基势垒高度（Φ_{BS}）有关。

2 结果与讨论

2.1 DBR结构参数的影响

首先分析DBR结构参数对器件吸收光谱和响应光谱的关联作用。可以调控的DBR结构参数包括介质层材料、周期和中心波长等。假设DBR高反射光谱带宽（$\Delta\lambda$）与TiN薄膜吸收光谱存在关联。$\Delta\lambda$表示为[40]

$$\frac{\Delta\lambda}{\lambda_0}=\frac{4}{\pi}\arcsin\left(\frac{n_H-n_L}{n_H+n_L}\right) \tag{6}$$

式中，λ_0为DBR中心波长，n_H和n_L分别为DBR介质层的高折射率和低折射率。高反射光谱带宽取决于n_H和n_L的比值以及λ_0的大小。设计了三种常见的DBR结构，其中，DBR-1由TiO_2和Al_2O_3组成，DBR-2由TiO_2和SiO_2组成，DBR-3由Ge和SiO_2组成，TiO_2和Ge作为高折射率介质层，Al_2O_3和SiO_2作为低折射率介质层。Ge的折射率来源于文献[41]，其余材料的折射率来源于文献[22]。多层薄膜结构的反射光谱和吸收光谱可通过光学传输矩阵模拟计算得到。表1列出了三种DBR结构介质层在1 300 nm处的折射率和模拟计算所使用的厚度。介质层折射率和厚度之间的关系理论上满足$\lambda_0/4=n_Hd_H=n_Ld_L$，$d_H$和$d_L$分别为高折射率和低折射率介质层厚度。图2（a）所示为各种DBR结构反射光谱，DBR中心波长为1 300 nm，周期数为8。三种DBR结构的高反射光谱带宽分别为284 nm、413 nm和850 nm。DBR-3结构中Ge和SiO_2的高折射率比显著拓宽了高反射光谱带宽。图2（b）所示为采用不同DBR结构热电子光电探测器的反射光谱，在DBR中心波长附近都形成了反射凹谷，特别是采用DBR-3的器件低反射光谱更宽，有利于减少入射光损耗，提高TiN薄膜宽带吸收率。图2（c）所示为采用不同DBR结构热电子光电探测器TiN薄膜的吸收光谱。所有器件TiN薄膜的最高吸收率均大于99.0%。TiN薄膜吸收光谱FWHM分别为345 nm、479 nm和906 nm，与DBR结构的高反射光谱带宽变化规律一致。图2（d）所示为热电子光电探测器除TiN薄膜之外的附加吸收光谱。器件反射率（Reflection）、TiN薄膜吸收率（$\mathrm{Absorption_{TiN}}$）和附加吸收率（$\mathrm{Absorption_{Parasitic}}$）之间的关系为：$\mathrm{Reflection+Absorption_{TiN}+Absorption_{Parasitic}}=1$。尽管Ge在近红外波段具有较强吸收系数，但因其作为DBR结构置于TiN之后，因此，除TiN之外各层薄膜在器件低反射光谱带宽内的附加光吸收比较弱。表明采用高折射率比的介质层构成DBR是实现热电子光电探测器宽带高吸收率的有效途径。

表 1 不同 DBR 结构中介质层在 1300 nm 处的折射率和相应厚度

Table 1 Refractive indices and corresponding thicknesses of the dielectric layers at 1300 nm with different DBR architectures

Type	n_H	n_L	d_H/nm	d_L/nm
DBR-1	2.40	1.70	135	190
DBR-2	2.40	1.45	135	225
DBR-3	4.25	1.45	75	225

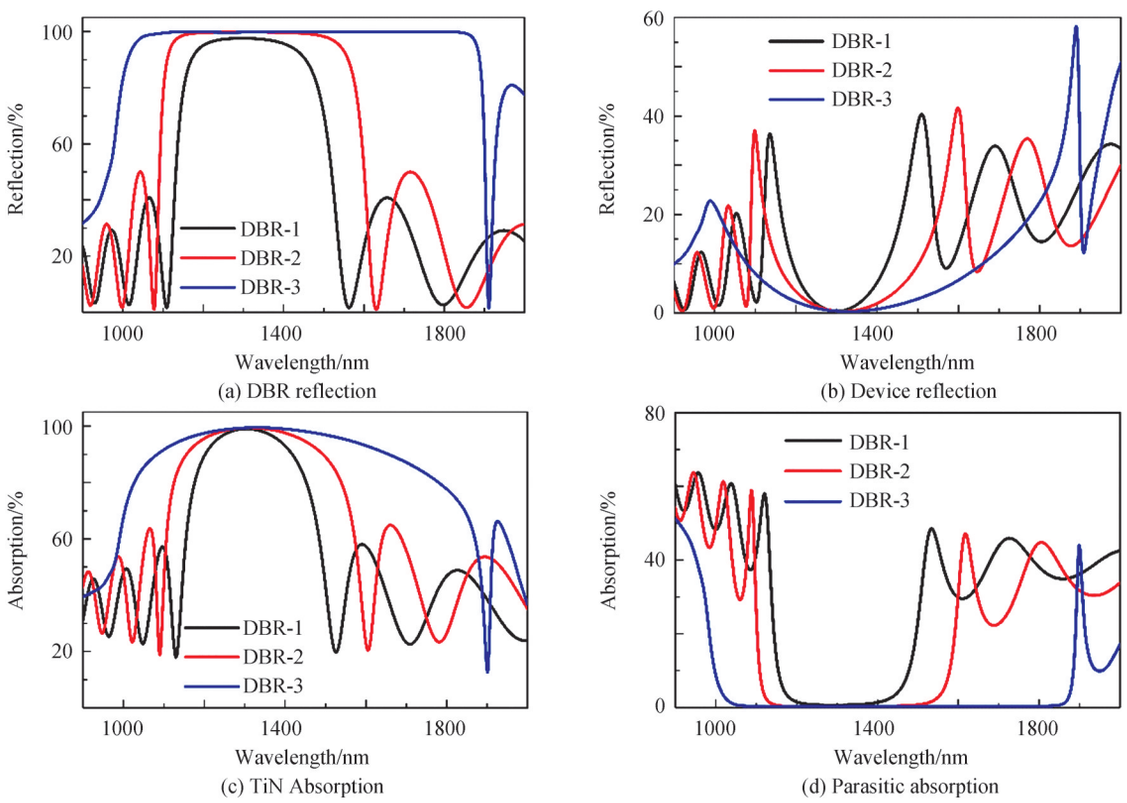

图 2 不同 DBR 结构及器件的反射光谱和吸收光谱

Fig. 2 Reflection and absorption spectra of various DBR structures and devices

由式(4)和(5)可计算得到不同波长的入射光对应的热电子能量分布。图 3 所示为 1 000 nm 和 1 800 nm 波长的入射光产生的热电子能量分布曲线。虚线表示 TiN/TiO_2肖特基势垒(0.37 eV)。能量高于肖特基势垒的热电子比例与入射光的能量和 TiN/TiO_2之间的势垒高度有关。入射光能量越高(波长越短)产生的高能热电子就越多,能量大于肖特基势垒的热电子比例越大,热电子穿过 TiN/TiO_2肖特基势垒注入到 TiO_2薄膜的概率越高。

根据式(2)和(3)可分别得到 TiN 薄膜中热电子的产生率和输运概率。图 4(a)和(b)分别显示了采用 DBR-3(中心波长为 1 300 nm,周期为 8)器件的 TiN 薄膜中热电子分布归一化产生率和输运概率。其中,MgF、ITO、TiO_2、TiN 的厚度分别为 100 nm、30 nm、10 nm 和 10 nm。结果表明,尽管低能量入射光(长波长)具有较高的产生率,但由于大部分热电子能量低,因此能够输运到达 TiN/TiO_2肖特基势垒界面的概率较低,能够越过肖特基势垒的热电子也就较少。假设入射光强按波长均匀分布(1 mW/cm^2),根据式(1)可进一步计算得到热电子光电探测器的响应度。图 4(c)所示为相应器件的响应光谱,峰值响应度为 29.2 mA/W,FWHM 为 866 nm。由此可见采用高折射率比的介质层构成 DBR 不仅扩宽了吸收光谱也拓宽了响应光谱,同时获得了高吸收率和高响应度。

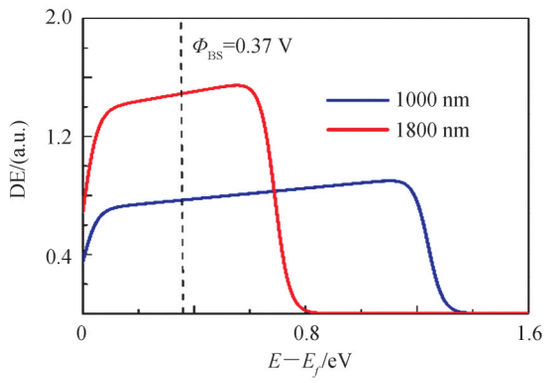

图3　波长为1000 nm和1800 nm的入射光产生的热电子能量分布曲线

Fig. 3　Energy distributed curves of the generation hot electrons with 1000 nm and 1800 nm incident light

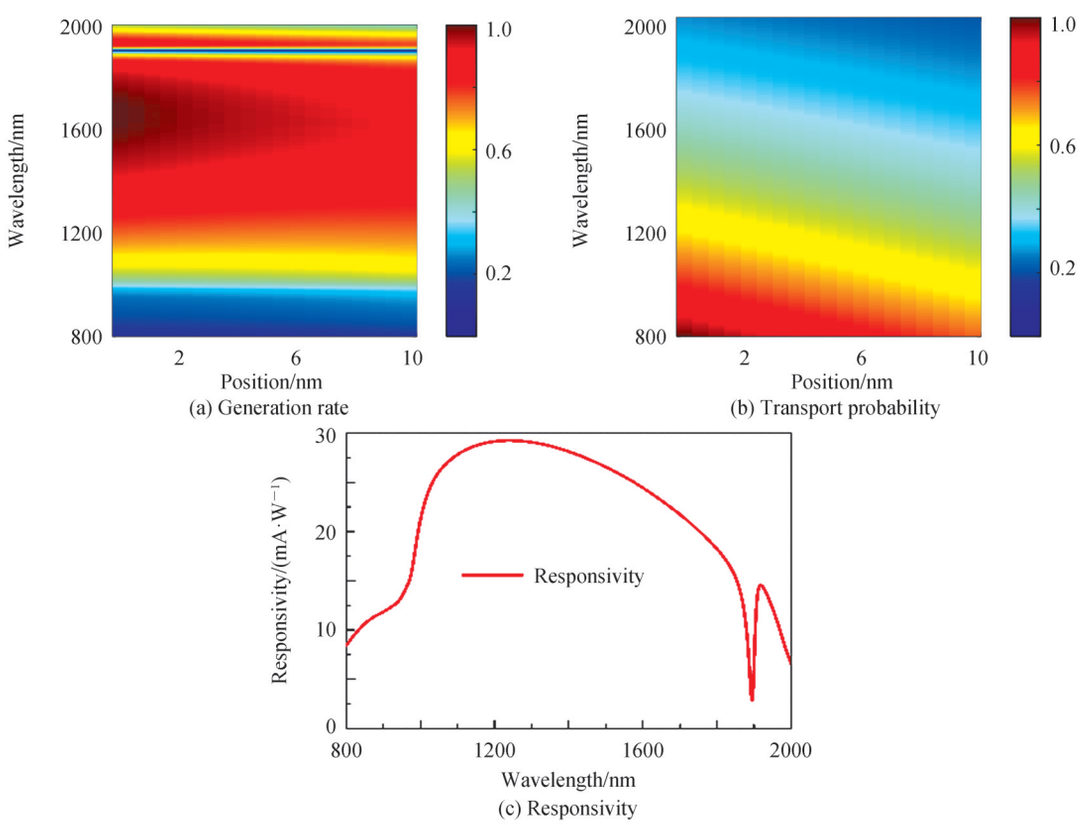

图4　TiN薄膜中电子产生率和输运概率的分布以及相应器件的响应光谱

Fig. 4　Generation rate and transport probability distributed in the TiN thin films and corresponding device response spectra

进一步探讨了DBR周期对TiN薄膜吸收率和器件响应度的影响。图5(a)为不同DBR周期对应的TiN薄膜吸收光谱。由于增加DBR周期可以提高DBR的反射率，更多的入射光被DBR反射回来被TiN所吸收，因此可以显著增强TiN薄膜的吸收率。图5(b)所示为器件响应光谱与DBR周期的关系。随着DBR周期的增加，得益于TiN薄膜吸收率的提高，器件响应度也明显增强。当DBR周期为5时，吸收率和响应度达到最大值，在1 310 nm波长处的吸收率和响应度分别为99.4%和29.0 mA/W，而在1 550 nm波长处则分别为95.3%和25.6 mA/W。采用较小的DBR周期仍然能保持较高吸收率和响应度，有利于减少器件厚度和缩减制备过程。

DBR中心波长与塔姆等离激元共振波长存在十分强的关联。塔姆等离激元产生的条件为[42]

$$\varphi_M+\varphi_{DBR}=2k\pi \quad k=0,1,2,\ldots \tag{7}$$

式中，φ_M和φ_{DBR}分别为金属薄膜和DBR结构的反射相位。进一步分析了DBR中心波长对TiN薄膜吸收光谱和器件响应光谱的影响。图6(a)和(b)所示分别为不同DBR中心波长对应的TiN薄膜吸收光谱和器件响应光谱。随着DBR中心波长的增加，塔姆等离激元共振波长也随之增大[16]。因此，吸收光谱和响应光谱范围发生红移。当DBR中心波长从1 150 nm增加到1 350 nm时，吸收光谱的FWHM从904 nm拓宽至950 nm，峰值吸收率由98.6%提高至99.6%。随着DBR中心波长的增大，器件响应光谱FWHM也得以提升，从884 nm增加至903 nm。而峰值响应度则由29.5 mA/W下降至29.1 mA/W。尽管DBR中心波长红移可以提高TiN薄膜吸收率，但由于长波长产生的热电子能量低，因此器件的内量子下降，导致响应度略微下降。改变DBR中心波长为调控热电子光电探测器吸收光谱和响应光谱范围提供了一种可行的策略。

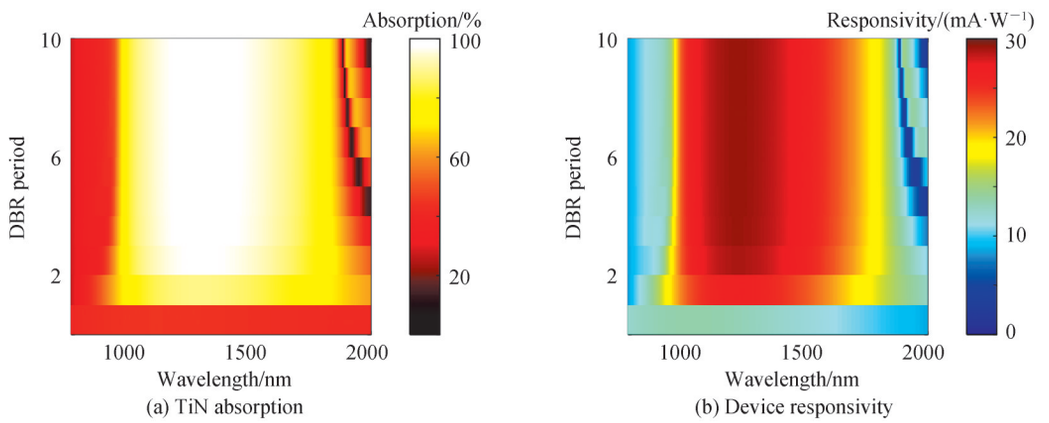

图5 不同DBR周期对应的TiN薄膜吸收光谱和器件响应光谱

Fig. 5 Absorption spectra of TiN thin films and device response spectra with various DBR period

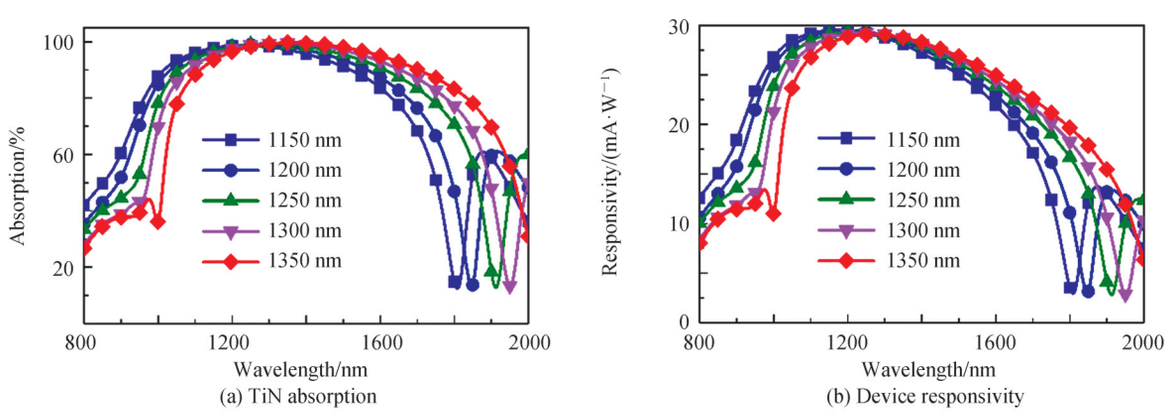

图6 不同DBR中心波长对应的TiN薄膜吸收光谱和器件响应光谱

Fig. 6 Absorption spectra of TiN thin films and device responsivity with different DBR central wavelengths

2.2 薄膜厚度的影响

TiN薄膜的吸收光谱与TiN薄膜厚度的关系如图7(a)所示。TiN薄膜的吸收率首先随TiN薄膜厚度的增加而增大。进一步增加TiN薄膜厚度，峰值吸收率维持在较高数值(90.0%以上)。图7(b)所示为不同TiN薄膜厚度对应的器件响应光谱。器件响应光谱随TiN薄膜厚度的变化趋势基本上与TiN薄膜吸收光谱的变化趋势一致。TiN薄膜为10 nm时，峰值吸收率为99.5%，峰值响应度达到最高值为29.2 mA/W。而TiN薄膜为13 nm时，峰值吸收率达到最大值为99.8%，峰值响应度下降为28.8 mA/W。TiN薄膜的厚度对热电子探测器的光电性能起着至关重要的作用。增大TiN薄膜厚度有利于提高吸收率，然而热电子的散射几率也随之增强，散射过程能量的损失导致热电子越过肖特基势垒的几率下降。

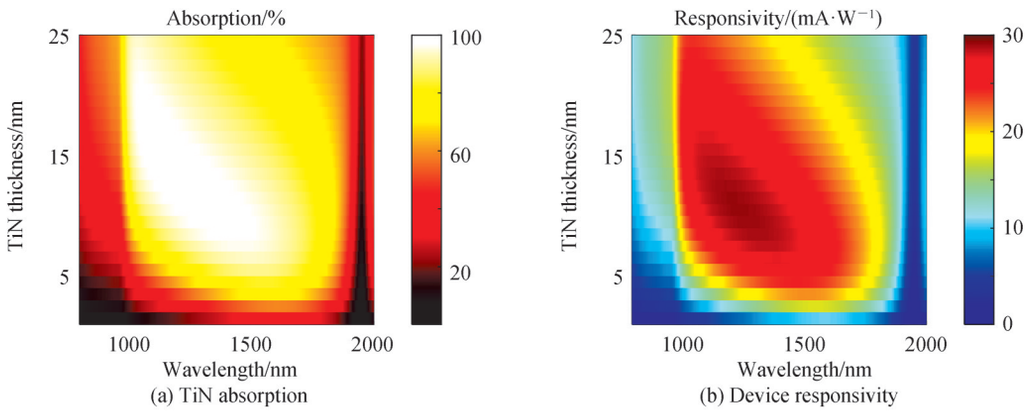

图7　不同TiN薄膜厚度对应的TiN薄膜吸收光谱和器件响应光谱

Fig. 7　Absorption spectra of TiN thin films and device responsivity spectra with various TiN thicknesses

为了进一步降低入射光损耗，提高TiN薄膜的吸收率，分析常见的低折射率MgF减反射层对器件吸收率和响应度的影响作用。图8(a)和(b)所示分别为不同MgF减反射层厚度对应的TiN薄膜吸收光谱和器件响应光谱。MgF减反射层厚度对热电子光电探测器的光电性能也有一定影响。随着MgF厚度的增加，器件在长波长处的吸收率和响应度都得以提高。当MgF厚度从0增加到200 nm时，吸收光谱和响应光谱的FWHM分别提升47 nm和81 nm。随着MgF厚度的增加，峰值吸收率和峰值响应度略有下降。引入MgF减反射层，对入射光产生光学干涉作用，可以调控TiN薄膜的吸收光谱。

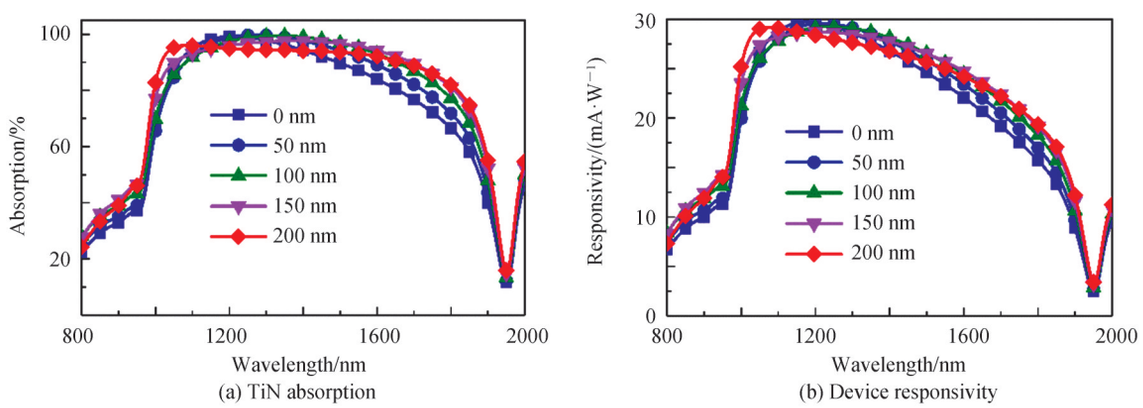

图8　不同MgF减反射层厚度对应的TiN薄膜吸收光谱和器件响应光谱(TiN薄膜厚度为10 nm)

Fig. 8　Absorption spectra of TiN thin films and device responsivity spectra as a function of MgF anti-reflectance layer thickness (the thickness of TiN thin films is 10 nm)

2.3　入射光偏振态的影响

不同入射光偏振态以及入射角都对光学传输矩阵有直接影响，因此也与器件的吸收率有关联作用，进而影响器件响应度。图9(a)和(b)分别为TE偏振和TM偏振入射光不同入射角对应的TiN薄膜吸收光谱。当入射角从0增加至30°时，塔姆等离激元仍然能够被激发，TiN薄膜的峰值吸收率随之下降。入射角为30°时，TE偏振对应的TiN薄膜峰值吸收率超过70.0%，略高于TM偏振的值。图10(a)和(b)分别为TE偏振和TM偏振器件响应光谱与不同入射角的关系。随着入射角从0增加至30°，TiN薄膜吸收率下降，器件响应度也随之下降。入射角为30°时，TE偏振和TM偏振对应的器件峰值响应度均超过20 mA/W，TE偏振的响应光谱FWHM比TM偏振的更宽，达到978 nm。这一差异可能来源于TiN薄膜对于TE偏振和TM偏振的二向色性[43]。TE偏振和TM偏振峰值吸收波长和峰值响应波长都随入射角增大而发生蓝移，与文献报道的结果一致[15,44]。

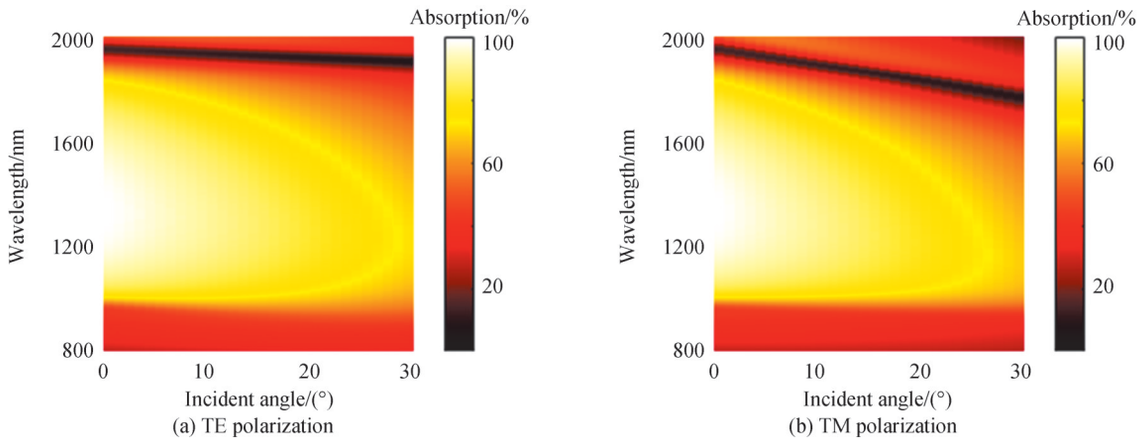

图 9 TE偏振和TM偏振不同入射角对应的TiN薄膜吸收光谱

Fig. 9 Absorption spectra of TiN thin films with different incident angles for the TE polarization and TM polarization

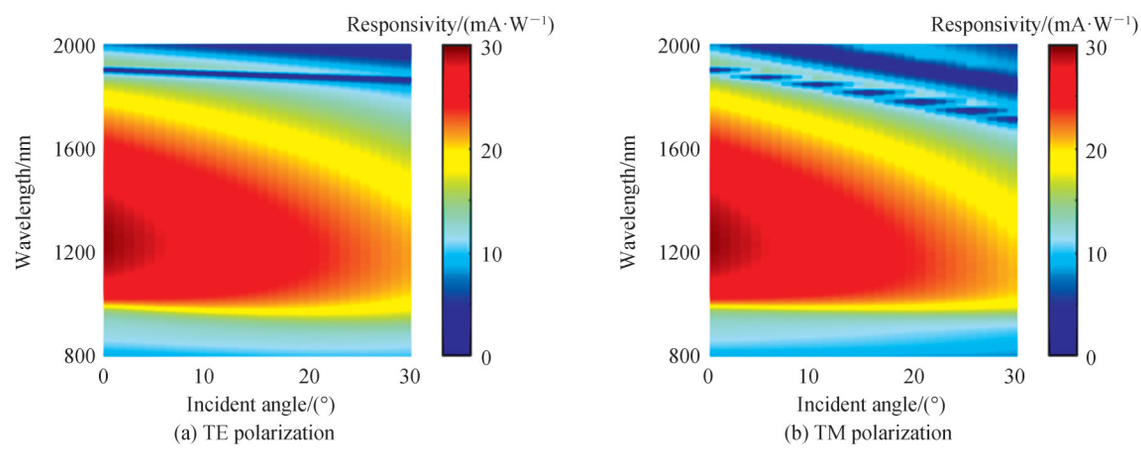

图 10 TE偏振和TM偏振器件响应度与不同入射角的关系

Fig. 10 Device responsivity as a function of incident angles with the TE polarization and TM polarization

3 结论

本文提出了一种基于TiN/TiO_2肖特基势垒和TiN/DBR塔姆等离激元的宽带近红外热电子光电探测器多层薄膜结构。从理论上研究了DBR结构参数(介质层、周期、中心波长等)对TiN薄膜吸收率和器件响应度的影响。研究结果表明,Ge/SiO_2的高折射率比拓宽了DBR的高反射光谱带宽,从而扩展了TiN薄膜吸收光谱和器件响应光谱的FWHM,并获得高吸收率和高响应度。通过调控DBR结构参数、TiN薄膜厚度和MgF减反射层厚度,可获得高于29.0 mA/W的响应度和约900 nm的响应光谱FWHM。本研究可为高性能宽带近红外热电子光电探测器的设计和制备提供新思路。

参考文献

[1] SHI Linlin, CHEN Keqiang, ZHAI Aiping, et al. Status and outlook of metal - inorganic semiconductor - metal photodetectors[J]. Laser & Photonics Reviews, 2021, 15(1): 2000401.

[2] HU Weida, LI Qing, CHEN Xiaoshuang, et al. Recent progress on advanced infrared photodetectors[J]. Acta Physica Sinica, 2019, 68(12): 120701.
胡伟达, 李庆, 陈效双, 等. 具有变革性特征的红外光电探测器[J]. 物理学报, 2019, 68(12): 120701.

[3] WANG Peng, XIA Hui, LI Qing, et al. Sensing infrared photons at room temperature: from bulk materials to atomic layers [J]. Small, 2019, 15(46): 1904396.

[4] LIU Yan, SUN Tian, MA Weiliang, et al. Highly responsive broadband black phosphorus photodetectors[J]. Chinese Optics Letters, 2018, 16(2): 020002.

[5] FENG Guobin, ZHANG Jianmin, YANG Pengling, et al. Responsivity variation with temperature of uncooled mid-infrared HgCdTe photoconductive detector[J]. Acta Photonica Sinica, 2013, 42(7): 787-791.

冯国斌, 张检民, 杨鹏翎, 等. 室温中红外HgCdTe光导探测器响应率的温度特性[J]. 光子学报, 2013, 42(7): 787-791.

[6] BRONGERSMA M L, HALAS N J, NORDLANDER P. Plasmon-induced hot carrier science and technology[J]. Nature Nanotechnology, 2015, 10(1): 25-34.

[7] TAGLIABUE G, DUCHENE J S, ABDELLAH M, et al. Ultrafast hot-hole injection modifies hot-electron dynamics in Au/p-GaN heterostructures[J]. Nature Materials, 2020, 19(12): 1312-1318.

[8] LAO Yanfeng, PERERA A G U, LI L H, et al. Tunable hot-carrier photodetection beyond the bandgap spectral limit[J]. Nature Photonics, 2014, 8(5): 412-418.

[9] HOU Y, LIANG H, TANG A, et al. Hot-electron photocurrent detection of near-infrared light based on ZnO[J]. Applied Physics Letters, 2021, 118(6): 063501.

[10] XIAO Hongbin, LO Shucheng, TAI Yihsin, et al. Spectrally selective photodetection in the near-infrared with a gold grating-based hot electron structure[J]. Applied Physics Letters, 2020, 116(16): 161103.

[11] SOBHANI A, KNIGHT M W, WANG Yumin, et al. Narrowband photodetection in the near-infrared with a plasmon-induced hot electron device[J]. Nature Communications, 2013, 4: 1643.

[12] LIANG Wenyue, XIAO Zheng, XU Haitao, et al. Ultranarrow-bandwidth planar hot electron photodetector based on coupled dual Tamm plasmons[J]. Optics Express, 2020, 28(21): 31330-31344.

[13] WANG Zhiyu, CLARK J K, HO Y L, et al. Hot-electron photodetector with wavelength selectivity in near-infrared via Tamm plasmon[J]. Nanoscale, 2019, 11(37): 17407-17414.

[14] SHAO Weijia, YANG Qianru, ZHANG Cheng, et al. Planar dual-cavity hot-electron photodetectors[J]. Nanoscale, 2019, 11(3): 1396-1402.

[15] YU Tong, ZHANG Cheng, LIU Huimin, et al. Planar, narrowband, and tunable photodetection in the near-infrared with Au/TiO_2 nanodiodes based on Tamm plasmons[J]. Nanoscale, 2019, 11(48): 23182-23187.

[16] ZHANG Cheng, WU Kai, GIANNINI V, et al. Planar hot-electron photodetection with tamm plasmons[J]. ACS Nano, 2017, 11(2): 1719-1727.

[17] TANG Haibin, CHEN Chihjung, HUANG Zhulin, et al. Plasmonic hot electrons for sensing, photodetection, and solar energy applications: a perspective[J]. The Journal of Chemical Physics, 2020, 152(22): 220901.

[18] CHEN Liang, MAO Sui, WANG Pu, et al. Visible light driven hot-electron injection by pd nanoparticles: fast response in metal - semiconductor photodetection[J]. Advanced Optical Materials, 2021, 9(1): 2001505.

[19] CLAVERO C. Plasmon-induced hot-electron generation at nanoparticle/metal-oxide interfaces for photovoltaic and photocatalytic devices[J]. Nature Photonics, 2014, 8(2): 95-103.

[20] WANG Kai, HU Haifeng, LU Shan, et al. Visible and near-infrared dual-band photodetector based on gold - silicon metamaterial[J]. Applied Physics Letters, 2020, 116(20): 203107.

[21] ZHAI Yusheng, LI Yupei, JI Jitao, et al. Hot electron generation in silicon micropyramids covered with nanometer-thick gold films for near-infrared photodetectors[J]. ACS Applied Nano Materials, 2020, 3(1): 149-155.

[22] WANG Jiaying, ZHU Yisong, WANG Wenhao, et al. Broadband Tamm plasmon-enhanced planar hot-electron photodetector[J]. Nanoscale, 2020, 12(47): 23945-23952.

[23] SAKHDARI M, HAJIZADEGAN M, FARHAT M, et. al. Efficient, broadband and wide-angle hot-electron transduction using metal-semiconductor hyperbolic metamaterials[J]. Nano Energy, 2016, 26: 371-381.

[24] SHINDE S L, ISHII S, NAGAO T. Sub-bandgap photodetection from titanium nitride/germanium heterostructure[J]. ACS Applied Materials & Interfaces, 2019, 11(24): 21965-21972.

[25] WANG Qilong, LI Yupei, ZHAI Yusheng, et al. Progress of surface plasmon enhanced near-infrared photodetector based on metal/Si Schottky heterojunction[J]. Infrared and Laser Engineering, 2019, 48(2): 0203002.
王琦龙, 李裕培, 翟雨生, 等. 等离激元增强金硅肖特基结近红外光电探测器进展[J]. 红外与激光工程, 2019, 48(2): 0203002.

[26] LIN Kengte, CHEN Hsuenli, LAI Yusheng, et al. Silicon-based broadband antenna for high responsivity and polarization-insensitive photodetection at telecommunication wavelengths[J]. Nature Communications, 2014, 5: 3288.

[27] CHEN Hongyu, LIU Hui, ZHANG Zhiming, et al. Nanostructured photodetectors: from ultraviolet to terahertz[J]. Advanced Materials, 2016, 28(3): 403-433.

[28] KHARITONOV A, KHARINTSEV S. Tunable optical materials for multi-resonant plasmonics: from TiN to TiON[J]. Optical Materials Express, 2019, 10(2): 513-531.

[29] NALDONI A, GULER U, WANG Zhuoxian, et al. Broadband hot-electron collection for solar water splitting with plasmonic titanium nitride[J]. Advanced Optical Materials, 2017, 5(15): 1601031.

[30] GONG Tao, MUNDAY J N. Materials for hot carrier plasmonics[J]. Optical Materials Express, 2015, 5(11): 2501-2512.

[31] ISHII S, SHINDE S L, JEVASUWAN W, et al. Hot electron excitation from titanium nitride using visible light[J].

ACS Photonics, 2016, 3(9): 1552-1557.
[32] PODDER S, PAL A R. Plasmonic visible-NIR photodetector based on hot electrons extracted from nanostructured titanium nitride[J]. Journal of Applied Physics, 2019, 126(8): 083108.
[33] ZHAO Shenyou, YIN Yanting, PENG Jun, et al. The importance of schottky barrier height in plasmonically enhanced hot-electron devices[J]. Advanced Optical Materials, 2021, 9(3): 2001121.
[34] ZHANG Cheng, WU Kai, ZHAN Yaohui, et al. Planar microcavity-integrated hot-electron photodetector [J]. Nanoscale, 2016, 8(19): 10323-10329.
[35] NG C, CADUSCH J J, DLIGATCH S, et al. Hot carrier extraction with plasmonic broadband absorbers[J]. ACS Nano, 2016, 10(4): 4704-4711.
[36] SUN Zhiguang, FANG Yurui. Hot-carrier generation from propagating plasmon in an antenna-spacer-mirror nanostructure[J]. Optics Letters, 2020, 45(15): 4357-4360.
[37] KATSIDIS C C, SIAPKAS D I. General transfer-matrix method for optical multilayer systems with coherent, partially coherent, and incoherent interference[J]. Applied Optics, 2002, 41(19): 3978-3987.
[38] KOVACS D A, WINTER J, MEYER S, et al. Photo and particle induced transport of excited carriers in thin film tunnel junctions[J]. Physical Review B, 2007, 76(23): 235408.
[39] WHITE T P, CATCHPOLE K R. Plasmon-enhanced internal photoemission for photovoltaics: theoretical efficiency limits[J]. Applied Physics Letters, 2012, 101(7): 073905.
[40] KASAP S O. Optoelectronics and photonics principles and practices[M]. Second Edition. England: Pearson Education Limited, 2012: 56-58.
[41] CIESIELSKI A, SKOWRONSKI L, PACUSKI W, et al. Permittivity of Ge, Te and Se thin films in the 200 - 1500 nm spectral range. Predicting the segregation effects in silver[J]. Materials Science in Semiconductor Processing, 2018, 81: 64-67.
[42] CHANG Chunchieh, CHEN Tingyun, LIN Tingwei, et al. Flexible and ultranarrow transmissive color filters by simultaneous excitations of triple resonant eigenmodes in hybrid metallic - optical tamm state Devices[J]. ACS Photonics, 2021, 8(2): 540-549.
[43] MIRZAEE S M A, LEBEL O, NUNZI J M. Simple unbiased hot-electron polarization-sensitive near-infrared photodetector[J]. ACS Applied Materials & Interfaces, 2018, 10(14): 11862-11871.
[44] LEE C, LEE Y K, PARK Y, et al. Polarization effect of hot electrons in tandem-structured plasmonic nanodiode[J]. ACS Photonics, 2018, 5(9): 3499-3506.

Near Infrared Hot Electrons Photodetectors Based on Tamm Plasmons

LUO Guoping, CHEN Xingyuan, HU Sumei, ZHU Weiling
(*School of Science*, *Guangdong University of Petrochemical Technology*, *Maoming*, *Guangdong* 525000, *China*)

Abstract: Photodetection is an important means of modern detection and intelligent sensing technology. Classical photodetectors are based on the interband transition of electrons in the semiconductor materials, and their maximum response wavelength depends on the optical band gap of the semiconductor materials. Only photons with energy higher than the band gap (wavelength less than the maximum response wavelength) can be detected. Infrared photoelectric detectors are widely used in military reconnaissance, aerospace remote sensing, astronomical observation, industrial detection, optical fiber communication, infrared imaging and other fields. Common infrared detectors are made of semiconductor materials with extremely narrow band gap, which are facing many problems such as complex processes, high costs and low operation temperature. Hot electrons photodetectors based on the internal photoelectric effect have attracted tremendous attention in the past decade due to its advantages such as overcoming the response limitation of the semiconductor band gap, fast response speed, working at room temperature and light polarization sensitivity. The main problem of hot electrons photodetectors is low device responsivity, especially in the near infrared regions. In recent years, numerous studies at home and abroad have demonstrated that optical means such as grating plasmons, Tamm plasmons and micro-cavity effect can effectively enhance the optical absorption of metal films in the hot electrons photodetectors, and further improve the device responsivity. The planar metal thin films / Distributed Bragg Reflector (DBR) Tamm plasmons have many advantages such as simple structure, low manufacturing cost, high absorption

efficiency. By changing the DBR structure parameters and metal thin films thickness, the resonance wavelength and maximum response wavelength can be adjusted. This structure provides an effective way to improve the absorption of hot electrons photodetectors, but the corresponding devices normally exhibits narrowband absorption and responsivity. The development of hot electrons photodetectors with broadband response characteristics is conducive to the expansion of its applications in optical fiber communication, photocatalysis, solar cells, solar water splitting and other fields. In view of broadband hot electrons photodetector, there are still some issues to be solved, such as narrow response spectra, low absorption efficiency, and low responsivity. TiN has high dielectric constants and excellent plasmons characteristics in the near infrared ranges. Moreover, the mean free path of hot electrons in the TiN thin films is about 50 nm, which is larger than the values of Au and Ag. Therefore, TiN is considered as potential candidate which can be used to achieve high performance broadband hot electrons photodetectors. In this study, we propose a multi-layer device architecture based on the TiN/TiO_2 Schottky barrier and the Tamm plasmons formed by the TiN/ DBR structure to achieve high-performance broadband near infrared hot electrons photodetectors. This architecture has the following characteristics: 1) The TiN/DBR Tamm plasmons with manipulating the DBR structural parameters are able to enhance broadband absorption of the TiN thin films and broaden the device response spectra; 2) The Schottky barrier of TiN/TiO_2 is only 0.37 eV, which will be beneficial to the transporting of low energy hot electrons; 3) The MgF anti-reflectance layer is used to reduce optical loss. Based on the optical transfer matrix and hot electrons emission theory, we firstly simulated the reflection and absorption spectra of the hot electrons photodetectors. Furthermore, we calculated the corresponding device responsivity. The simulation results show that with high refractive indices ratio dielectric layers, the DBR form by Ge/SiO_2 can effectively expand the absorption spectra of the TiN thin films and the device response spectra. The absorption of TiN thin films and device responsivity also can be largely enhanced. By adjusting the DBR structural parameters, such as dielectric layers, DBR period and the DBR center wavelength, the absorption spectra of TiN thin films and the responsivity spectra of the hot electrons devices can be regulated. We also discuss the influences of the thickness of TiN thin films and MgF anti-reflectance layer. The maximum absorption of the TiN thin films is 99.8%, and the maximum responsivity value of the optimized device is 29.2 mA/W. The full width at half maximum of the response spectra is about 900 nm. The simulation results indicate that as the incident angle increases from 0 to 30°, the Tamm state can still be excited, but the peak absorption of the TiN thin films and the device responsivity are decreased. The peak absorption and response wavelength under the TE polarization and TM polarization are both blue shifted with the increasing of incident angles. This multi-layer device architecture provides a new route to realize high-performance broadband near infrared hot electrons devices. Meanwhile, it is beneficial to expand the applications of hot electrons photodetectors.

Key words: Photodetectors; Hot electrons; Plasmons; Quantum efficiency; Thin films

OCIS Codes: 040.5160; 040.3060; 230.4170; 230.1480

Foundation item: National Natural Science Foundation of China (No. 12074441), the Natural Science Foundation of Guangdong Province, China (Nos. 2018A030307028, 2019A1515010916), the Research Foundation of Education Bureau of Guangdong Province, China (No. 2017KQNCX136), the Natural Science Foundation of Guangdong University of Petrochemical Technology, China (No. 2017rc20)